ISSN 1996-3343

Asian Journal of Applied Sciences

http://knowledgiascientific.com

Knowledgia SCIENTIFIC
A Place to Publish Outstanding Research

OPEN ACCESS Asian Journal of Applied Sciences

ISSN 1996-3343
DOI: 10.3923/ajaps.2016.159.169

Research Article
Effect of Zn Film Substrate Temperature on Optical, Structural and Vibrational Characteristics of Thermally Oxidized Zn Films

[1]K.U. Isah, [2]A.M. Ramalan, [1]U. Ahmadu, [1]S.O. Ibrahim, [3]J.A. Yabagi and [1]B.J. Jolayemi

[1]Department of Physics, School of Physical Sciences, Federal University of Technology, Minna, Nigeria
[2]University of Abuja, Abuja, Nigeria
[3]Ibrahim Badamasi Babangida University, Lapai, Nigeria

Abstract

Background: This study presents the effect of metallic Zn film substrate temperature on the optical, morphological and structural properties of thermally oxidized Zn films. **Materials and Methods:** Zinc oxide (ZnO) thin films were synthesised by thermal oxidation at 400°C of metallic zinc thin films deposited by vacuum thermal evaporation onto glass substrate at different substrate temperatures of room temperature 100 and 150°C. **Results:** The ZnO films show significant modification in morphology with different nanostructures at different Zn film precursor substrate temperature. The stoichiometric ratio between Zn and O atoms of the ZnO films synthesised at room temperature and 100°C metallic Zn films precursor substrate temperature had a large deviation from the ideal ratio of 1:1 and was closer to ideal at a Zn film precursor substrate temperature of 150°C giving $ZnO_{0.94}$. All the films exhibited preferred (011) orientation of wurtzite structure, with presence of Zn peaks that diminishes with increasing metallic Zn substrate temperature. The films had optical transmittance of 64-71% in the visible region with the transmission edge becoming sharper and the optical band gap improving from 2.35-3.30 eV with increase in substrate temperature. The characteristic wurtzite ZnO Raman peaks of E_2^{low} are observed at 106 cm^{-1} for the three samples showing a blue shift. The XRD and Raman analysis indicates identical crystal structures irrespective of Zn film precursor substrate temperature. **Conclusion:** The precursor Zn film substrate temperature show significant effect on morphology, nanostructure shape and stoichiometry of the ZnO films. The control of the growth morphology and stoichiometry of ZnO will have an impact on possible optoelectronic applications.

Key words: Zinc oxide, thermal oxidation, substrate temperature, surface morphology, Raman spectroscopy, XRD

Received: May 01, 2016 Accepted: August 12, 2016 Published: September 15, 2016

Citation: K.U. Isah, A.M. Ramalan, U. Ahmadu, S.O. Ibrahim, J.A. Yabagi and B.J. Jolayemi, 2016. Effect of Zn film substrate temperature on optical, structural and vibrational characteristics of thermally oxidized Zn films. Asian J. Applied Sci., 9: 159-169.

Corresponding Author: K.U. Isah, Department of Physics, School of Physical Sciences, Federal University of Technology, Minna, Nigeria

Competing Interest: The authors have declared that no competing interest exists.

Data Availability: All relevant data are within the paper and its supporting information files.

INTRODUCTION

Zinc oxide (ZnO) is as multifunctional semiconducting material with distinctive physical and chemical properties such as hardness, high chemical stability, high electrochemical coupling coefficient, broad range of radiation absorption and high photo stability[1]. Its broad band gap of 3.37 eV, high bond energy (60 meV) and high thermal and mechanical stability at room temperature makes it very attractive for use in electronics, optoelectronics and laser technology[2-4]. The piezo- and pyroelectric properties of ZnO makes it viable as a sensor, converter, energy generator and photocatalyst in hydrogen production[5,6]. Also its hardness, rigidity and piezoelectric constant makes it important material in the ceramics industry, while its low toxicity, biocompatibility and biodegradability make it a material of interest for biomedicine and in pro-ecological systems[7-9]. Another major area of its application is in fuel cell where it is used to make various parts like the electrodes (Transparent Conductive Oxide (TCO) films) and sometimes also as the fuel. It can also act as a photo catalyst in places like the solar cell[10]. The ZnO is classified a II-VI semiconductor, whose bonding is on the boundary between ionic and covalent semiconductors.

Several methods have been used to grow ZnO thin films including sol-gel, solvothermal, sputtering, spray pyrolysis and thermal oxidation[11]. Among common methods used to synthesise ZnO, thermal oxidation is a simple low-cost technique. The ZnO thin film can be synthesized by oxidizing metallic Zn at an elevated temperature in open air without the presence of a catalyst and carrier gas[12] which make it economically viable as it uses the oxygen from the air.

In this study, thermal oxidation of thermally evaporated metallic zinc (Zn) films deposited onto glass substrate under vacuum was used to synthesis ZnO thin films. The evolution of the morphological, microstructural, optical and vibrational properties of the ZnO films as a function Zn film substrate temperature were investigated using Field Emission Scanning Electron Microscope (FESEM), Atomic Force Microscope (AFM), x-ray diffraction (XRD), UV/vis spectroscopy and Raman spectroscopy.

MATERIALS AND METHODS

Metallic zinc (Zn) pellets (99.9%) were thermally evaporated onto corning 7059 glass substrate under vacuum from a molybdenum boat at three different substrate temperature (Room temperature, 100 and 150°C) at a vacuum pressure of 1.15×10^{-5} torr, constant deposition rate of 2 nm sec^{-1} and constant source to substrate distance of 8 cm using an EDWARD Auto306 thermal evaporator with FL 400 deposition chamber. The deposited metallic Zn precursor thin films were each oxidised at 400°C in open air under atmospheric pressure. A dwelling time of 120 min was adopted to oxidise the films. The oxidised samples were named T_{sub_RT}, $T_{sub\_100°C}$ and $T_{sub\_150°C}$ for metallic Zn precursor substrate temperatures at room temperature, 100 and 150°C respectively.

The morphology of the films were investigated using JEOL JSM-7600F Field Emission Scanning Microscopy (FESEM) equipped with an Aztec and INCA microanalysis system with 50 mm^2 silicon drift detector as well as INCA wave Wavelength Dispersive Spectrometer (WDS) system for identification and measurement of the elements and Atomic Force Microscope (AFM) using an XE-100 Park system attached with XE Series (SPM) Shidmadzu. The x-ray diffraction (θ-2θ) diagrams were recorded with 2θ scanning from 25-60°, in step size 0.040° and a constant countingtimes of 3.17 sec per step and the generator settings of 40 mA and 42 kV, with CuK_α of 1.5406 Å using a X'Pert' Powder PANALYTICAL Bruker D8 Advance Diffractometer. The optical and vibrational properties were investigated using Avantes UV-vis spectrophotometer (AVASPEC 2048) in the wavelength range 250-900 nm and ProRaman-L ENWAVE OPTRONICS Raman spectrometer with 750 nm wavelength, respectively.

RESULTS AND DISCUSSION

Surface morphology and compositional analysis: Figure 1 shows FESEM images showing evolution of sample surface morphology with substrate temperature. Nanoflaked-shapes were formed for sample T_{sub_RT} as seen in Fig. 1a. It shows a more compact and denser nanocrystallites, this may suggest a strong interaction between the impinging Zn atoms and the substrate at low substrate temperature, the strong interaction leads to high nuclei density and with attachment of adatoms as the nuclei grow. The aggregation of deposited atoms with little desorption from substrate surface, low adatom diffusion and shadowing effect at low substrate temperature leads to linear film growth and compact film[13].

At Zn substrate temperature of 100°C, the ZnO film show intersecting dendritic elongated nanowall texture with nanopores as shown in Fig. 1b. The crystallites are larger compared to T_{sub_RT} sample perhaps as a result of high adatom mobility to overcome self-shadowing effect resulting in the growth of large elongated crystallites[14]. For the oxidised Zn films deposited at Zn film substrate temperature of 150°C the microstructure evolved into nanoplatelets-like shape and a few of nanoarcs as shown in Fig. 1c. There is a significant

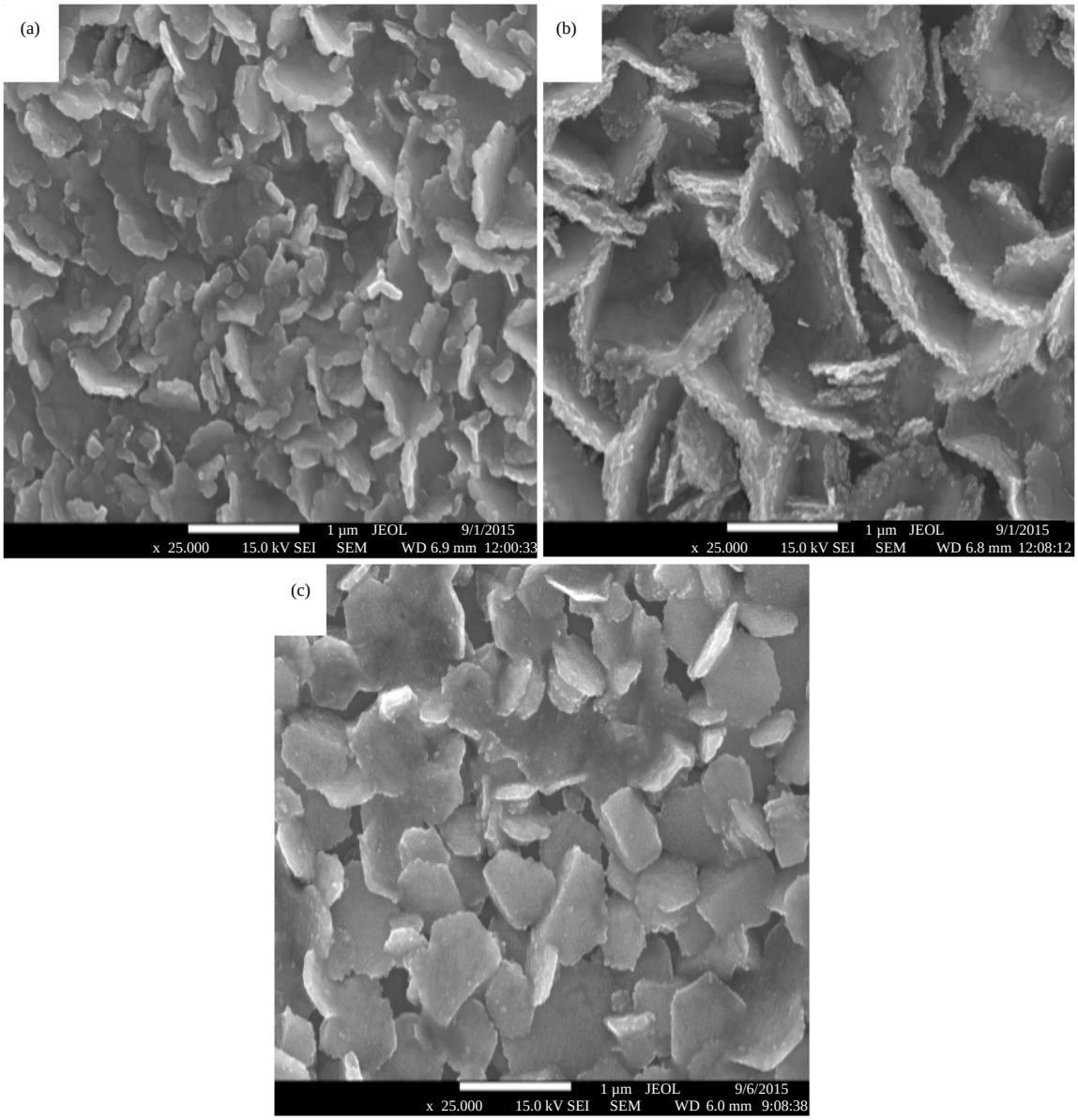

Fig. 1(a-c): FESEM images of ZnO films at same oxidation temperature of 400°C for different Zn film substrate temperature, (a) Room temperature, (b) 100°C and (c) 150°C

modification of ZnO film morphology showing different nanostructures at different Zn precursor substrate temperature. This implies the Zn precursor substrate temperature have a significant effect on the structure of ZnO, thus optimum Zn film substrate temperature is required for desired ZnO nanostucture. A wide range of nanostructures have been reported for ZnO, such as nanoneedles, nanowires and nanoflakes[15-17].

The grain sizes were determined from the SEM micrographs and shows increase from 82.95 nm for sample T_{sub_RT} to 181.66 nm for $T_{sub\_100°C}$ and subsequently decreased to 68.90 nm for $T_{sub\_150°C}$ sample.

The EDX spectra of the samples are given in Fig. 2, it shows only Zn and O. No other elements other than Zn and O are detected by the EDS analysis for all the samples.

The ZnO atomic ratio should be 50:50 from its chemical formula, however the EDS analysis revealed atomic ratios of 69.90:30.10 and 69.34:30.66 forming $ZnO_{0.43}$ and $ZnO_{0.44}$ for T_{sub_RT} and $T_{sub\_100°C}$ samples respectively, indicating a significant deviation from stoichiometry from deficiency of oxygen and presence of high amount of unoxidised Zn for these samples. This may be attributed to some inhibiting factors to the effective diffusion path for oxygen and thus proper oxidation of the films

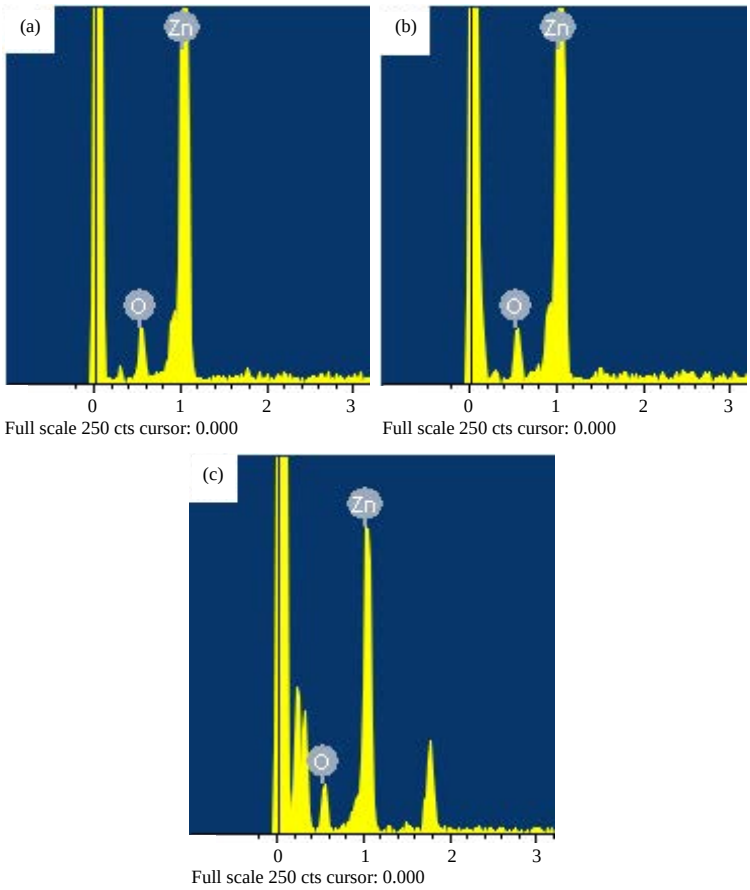

Fig. 2(a-c): EDX spectra of the ZnO samples for different Zn film substrate temperatures, (a) Room temperature, (b) 100°C and (c) 150°C

probably based on the microstructure of the Zn films form at the given Zn substrate temperature.

There is a considerably very low deviation in atomic percentages of Zn and O for the sample at Zn film substrate temperature of 150°C ($T_{sub\_150°C}$) with atomic Zn:O ratio of 51.56:48.44 and the formation of stoichiometry of $ZnO_{0.94}$, thus exhibiting a deviation of just 0.06 from actual ZnO stoichiometric ratio. This improvement in ZnO stoichiometry for $T_{sub\_150°C}$ may be due to the existence of more cleavages or grain boundaries, smaller particle size and more effective diffusion path for oxygen diffusion and reaction with metallic Zn film deposited at elevated Zn film substrate temperature. Thus the transformation of Zn into ZnO show a significant dependence on Zn film precursor substrate temperature. The results of the chemical composition, stoichiometry and grain size of the films are summarised in Table 1.

The film surfaces were scanned using AFM and Fig. 3 shows the 2D and 3D surface morphology of the films. Observed "Valley and hill-like" and thus columnar structure indicates preferential orientation of the nanocrystallites.

Table 1: Effects of Zn film substrate temperature on the chemical composition of ZnO thin films

	Chemical composition (%)				
Samples	Zn	O	ZnO_x	$D_{(011)}$ (nm)	R_a (nm)
T_{sub_RT}	69.90	30.10	$ZnO_{0.43}$	82.95	40.64
$T_{sub\_100°C}$	69.34	30.66	$ZnO_{0.44}$	181.66	81.38
$T_{sub\_150°C}$	51.56	48.44	$ZnO_{0.94}$	68.90	40.05

The average surface roughness R_a show a similar trend with crystallite size in Table 1. It shows an increase from 40.639 nm for T_{sub_RT} to 81.378 nm for sample $T_{sub\_100°C}$. This increase in roughness may be attributed to the nature of the Zn crystallites formed on substrate prior to the oxidation of the films during deposition process[18]. However, the surface roughness decreases at 150°C substrate temperature to 40.053 nm which may be attributed to the coalescence of crystal grains during the annealing processes due to the migration of grain boundaries as a result of stimulation under high temperature[19,20].

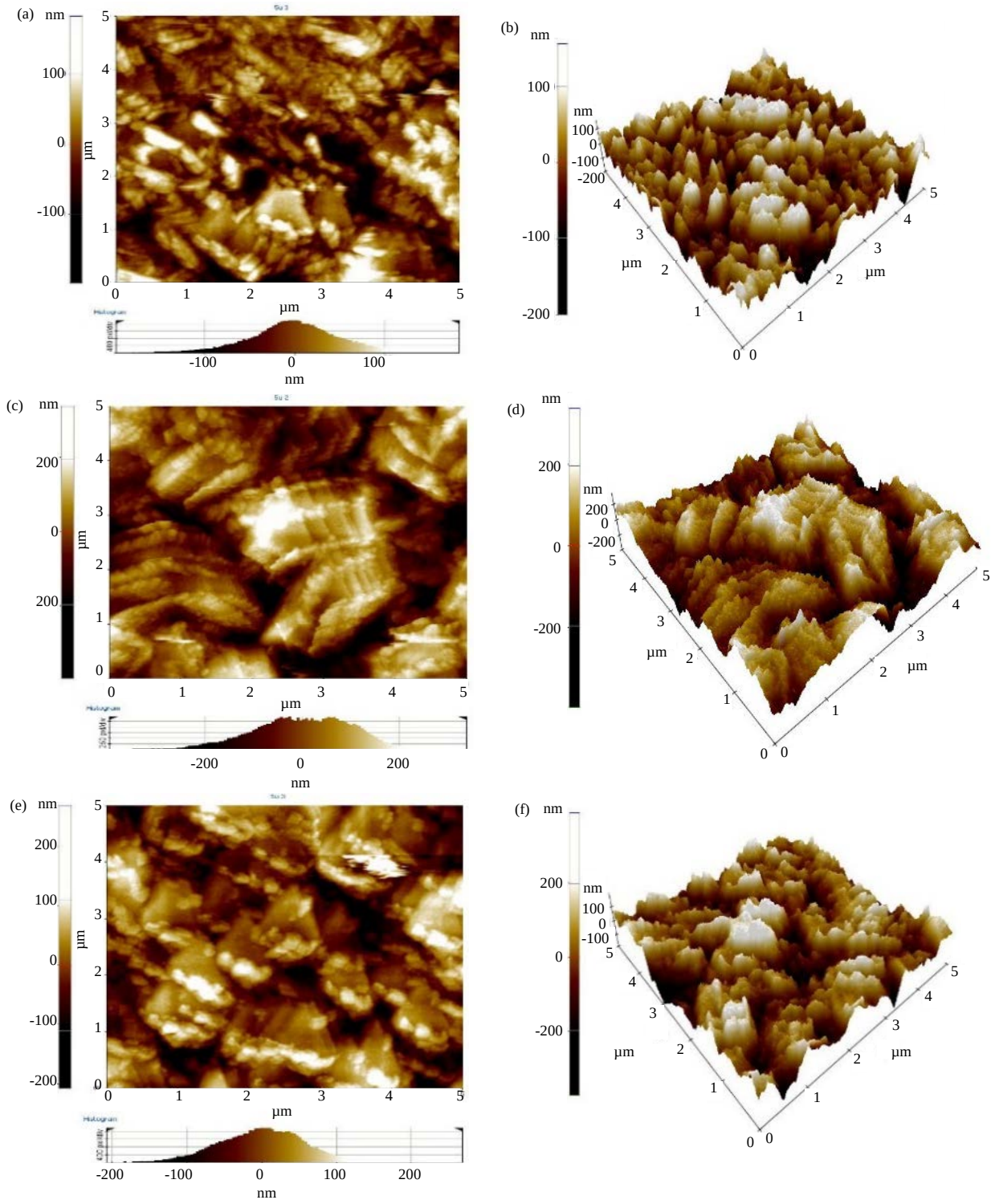

Fig. 3(a-f): 2D and 3D morphological images of the ZnO films for Zn substrate temperatures of (a and b) Room temperature, (c and d) 100°C substrate temperature and (e and f) 150°C

Structural properties: The XRD spectra of synthesised ZnO films at room, 100 and 150°C Zn film substrate temperature are given in Fig. 4.

The XRD spectra of the samples shows a mixed pattern of Zn and ZnO diffraction peaks. The diffraction peaks at values of 32.070, 34.470 and 36.470° correspond to (010),

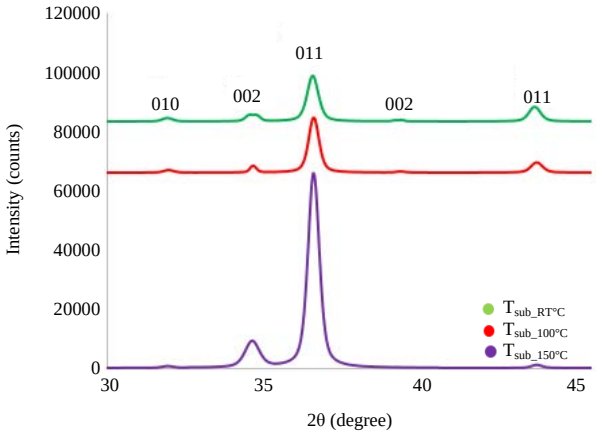

Fig. 4: XRD patterns of ZnO thin film samples at different Zn film substrate temperature: Room temperature (RT), 100°C and 150°C

Table 2: Structural parameters of the ZnO at different Zn film substrate temperatures

Samples	2θ (°)	β (°)	a (Å)	c (Å)	c/a	D (nm)	δ (10^{14} lines m^{-2})	$TC_{(011)}$	L (Å)
T_{sub_RT}	36.3734	0.3654	3.0022	5.1995	1.732	27.17	13.5	1.85	1.834
$T_{sub\_100°C}$	36.3777	0.3542	2.9991	5.1942	1.732	73.11	1.87	2.40	1.834
$T_{sub\_150°C}$	36.3463	0.3936	3.0083	5.2100	1.732	52.68	3.65	2.80	1.834

(002) and (011) planes respectively indexed to a hexagonal (wurtzite) ZnO structure (ICSD 169463). The observed (002) and (011) peaks around 39.270 and 43.350° belongs to Zn hexagonal system of space group P63/mmc (ICSD 52259). The identified peaks which are associated with Zn hexagonal results from un-oxidised zinc atoms during the oxidation process[21]. The films are preferentially oriented along (011) direction rather than the usual (002) orientation. The (011) and (002) ZnO diffraction peaks are sharper and more intense for the $T_{sub\_150°C}$ sample with almost complete disappearance of Zn peaks. This shows dependence of the dominant texture of the ZnO film on metallic Zn film precursor substrate temperature. The structural parameters of the samples were evaluated from the XRD figures and data, the results are summarised in Table 2.

The average crystallite size of the ZnO thin films were deduced using Debye Scherrer's formula[22]:

$$D = \frac{0.9\lambda}{\beta \cos\theta}$$

where, β is full width at half maximum (FWHM), k = 0.9 is the size factor, θ is diffraction angle at which the maximum intensity was observed, λ is wavelength of the x-rays used (1.54060) and D is crystallite size respectively.

The crystallite size from the Scherrer formula is between 27.17 and 73.11 nm as given in Table 2, which though show a similar trend is lower than the determined values from SEM images that lies between 68.90 and 181.66 nm. The SEM visualization allows only seeing grains, which are constituted of more or less disordered atoms and particles, while XRD gives the coherence length of atoms[23], thus the difference.

The dislocation density (δ), a measure of the amount of defects in the sample is defined as the length of dislocation lines per unit volume of the crystal was determined from Williamson and Smallman's formula[24]:

$$\delta = \frac{n}{D^2}$$

where, n is a factor, which when equal to unity gives the minimum dislocation density and D is the average crystallite size.

There is a decrease in dislocation density from 13.5×10^{14} to 1.87×10^{14} lines m^{-2} with increase in Zn film precursor substrate temperature from room temperature (sample T_{sub_RT}) to 100°C (sample $T_{sub\_100°C}$) which then increase to 3.65×10^{14} lines m^{-2} for Zn substrate temperature of 150°C (sample $T_{sub\_150°C}$), while the grain size show an increase in crystallite size from 27.17 nm for T_{sub_RT} to 73.11 nm for $T_{sub\_100°C}$ and a drop in size to 52.68 nm for $T_{sub\_150°C}$. It is thus observed that increase in grain size results in decrease in the dislocation density as can be seen in Table 2.

The Texture Coefficient (TC) represents the texture of a particular plane, whose deviation from unity implies the preferred growth. The value TC (hkl) = 1 represents films with randomly oriented crystallites, while higher values indicate the abundance of grains oriented in a given (hkl) direction, TC, is given[25]:

$$TC_{hkl} = \frac{I_{hkl} / I_{o(hkl)}}{N^{-1}\sum I_{hkl} / I_{o(hkl)}}$$

The texture coefficient for the (011) plane, the most prominent orientation of the samples have values greater than unity, between 1.88 for sample T_{sub_RT} and 2.8 for $T_{sub\_150°C}$, this shows the nanocrytals have increasing texture in this orientation and large number of crystallites are oriented with the (011) planes parallel to substrate surface[26] with increase in Zn film substrate temperature.

The obtained values of lattice parameters a and c of the samples given in Table 2 are less than the ideal values of the hexagonal unit cell of 3.2495 and 5.2069 Å, respectively and the ratio of the lattice parameter c/a had a constant value of ≈1.732 for all the samples which shows a deviation of 0.099 from 1.633 of the ideal wurtzite structure[27]. These deviations are due to defects in the lattice structure.

The nearest-neighbor Zn-O bond length L along the c-direction was determined from the lattice parameters using[28]:

$$L = \left[\frac{a^2}{3} + \left(\frac{1}{2} - u\right)^2 c^2\right]^{1/2}$$

where, the parameter u is the length of the bond parallel to the c axis is given by:

$$u = \frac{a^2}{3c^2} + 0.25$$

The values obtained were ≈1.834 Å for each samples. This is less than the theoretical Zn-O bond length of 1.993 Å along c-axis and 1.973 Å in the other three directions of the tetrahedral arrangements of the nearest neighbours determined from bond overlap population between Bloch functions on an atomic basis expansion[29] an indication of the planes being more closely packed than ideal. The values of the texture coefficients and the Zn-O bond lengths are also given in Table 2.

The deviation in c/a ratio and bond length L from the ideal wurtzite crystal is probably due to lattice stability and ionicity[27]. However, the same numerical values of c/a and L obtained for all the samples indicates identical crystal structures for the synthesised ZnO films irrespective of Zn precursor substrate temperature.

Optical properties: The optical transmittance spectra of the samples is shown in Fig. 5, it shows an increase in optical transmittance with increase in Zn precursor substrate temperature, with sample $T_{sub\_150°C}$ showing highest transmittance of 77% in the visible region.

The high amount of unoxidised Zn films in samples T_{sub_RT} and $T_{sub\_100°C}$ act as scattering centres for light accounting for lower optical transmittance of 64 and 71% respectively. The $T_{sub\_150°C}$ sample also show a sharper transmission edge compared to the other samples as a result of its better stoichiometry.

The ZnO being a direct band gap semiconductor, the optical band gap E_g of the samples were deduced from the relation:

$$(ahv) = B(hv - E_g)^{1/2}$$

where, α is absorption coefficient at photon energy hv and B is a constant. The optical band gap E_g were determined by extrapolating the linear part of $(\alpha hv)^2$ versus hv to hv axis as shown in Fig. 6.

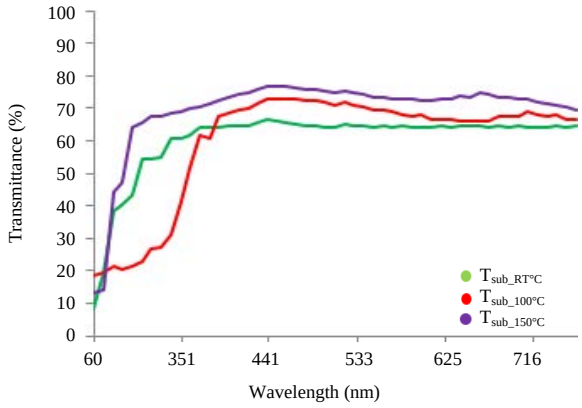

Fig. 5: Transmittance spectra of the ZnO films samples at different Zn film substrate temperatures

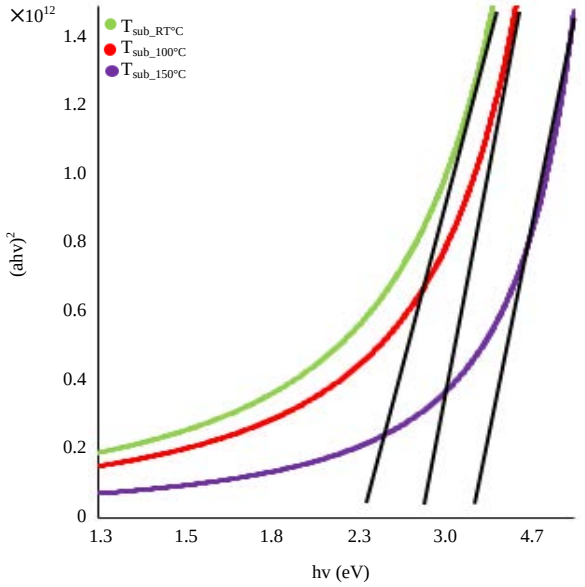

Fig. 6: Plots of $(\alpha hv)^2$ versus photon energy (hv) of the ZnO films at different Zn film substrate temperature

The band gaps given in Table 3 are in the range of 2.35 and 3.30 eV. The lower values of E_g for T_{sub_RT} and $T_{sub\_100°C}$ samples is associated with defects between the bands and attributable to greater density of states near the conduction band determined by oxygen vacancies[5].

The Urbach behaviour of the absorption edge based on the spectral behaviour of the absorption coefficient α is given by Urbach[30]:

$$\alpha = \alpha_0 \exp\left(\frac{hv}{E_u}\right)$$

where, α_o is a constant and E_u is the Urbach energy which is constant or weakly dependent on temperature and interpreted as the width of the tail of localized states in the band gap. It characterizes the degree of the absorption edge smearing resulting from crystalline lattice disordering due to structural peculiarities and those induced by external factors[31].

The increase exponentially of the absorption coefficient in the region of the absorption edge results from the transitions between the tails of density-of-states in the valence band and the conduction band, the shape and size of these tails is a function of the presence of different types of disordering[32].

The variation of lnα versus photon energy is given in Fig. 7.

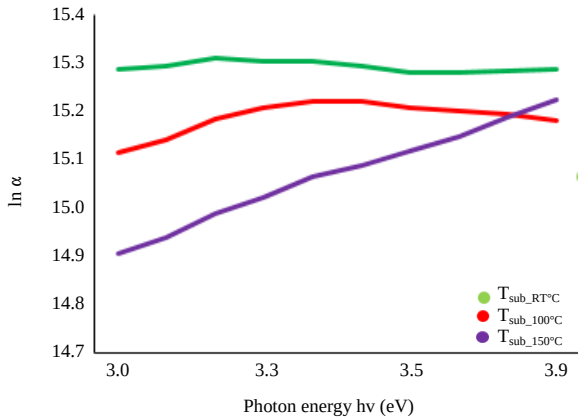

Fig. 7: Plots of lnα versus photon energy hv of the ZnO film samples at different Zn film substrate temperatures

Table 3: Transmittance, optical band gap and Urbach energy of the samples

Samples	T (%)	E_g (eV)	E_u (eV)
T_{sub_RT}	64	2.35	-
$T_{sub\_100°C}$	71	2.80	3.75
$T_{sub\_150°C}$	77	3.30	4.12

The values of E_u determined from the plot in Fig. 7 are given in Table 3. For sample T_{sub_RT} the plot is almost a horizontal line and thus its E_u was not determined. However, it increased from 3.75 eV for $T_{sub\_100°C}$ to 4.12 Ev in the case of $T_{sub\_150°C}$ sample. This may result from the relaxation of distorted bonds[33]. It shows a direct relation with the optical band gap.

Raman spectroscopy: The Raman spectrum of the samples are shown in Fig. 8. Raman frequencies of the fundamental optical modes in ZnO are E_2^{low} = 101 cm^{-1}, E_2^{high} = 437 cm^{-1}, 1 (TO) = 380 cm^{-1}, 1 (LO) = 574 cm^{-1}, 1 (TO) = 407 cm^{-1} and 1 (LO) = 583 cm^{-1} [34].

The characteristic wurtzite ZnO peaks of E_2^{low} are observed at 106 cm^{-1} for the three samples showing a blue shift, while the characteristic wurtzite ZnO E_2^{high} non-polar optical phonons were red shifted to 434 cm^{-1} for T_{sub_RT} and 432 cm^{-1} for $T_{sub\_100°C}$ and $T_{sub\_150°C}$ samples respectively. The 418 cm^{-1} corresponds to E_1 (TO) with a red shift of 5 cm^{-1} while peaks at 564 for T_{sub_RT}/$T_{sub\_150°C}$ and 566 for $T_{sub\_100°C}$ correspond to A_1 (LO) which are also red shifted. Raman peaks between 570 and 590 cm^{-1} are due to structural defects attributed to oxygen vacancy, Zn insterstitial and their combination[35]. The modes at 198/204 and 328 cm^{-1} are assigned as $2E_2^{low}$ and $E_2^{high} - E_2^{low}$ modes, respectively[36] and the peaks[37] at 548/550 are due to $2B_1^{low}$. The other observed peaks may be from the substrate.

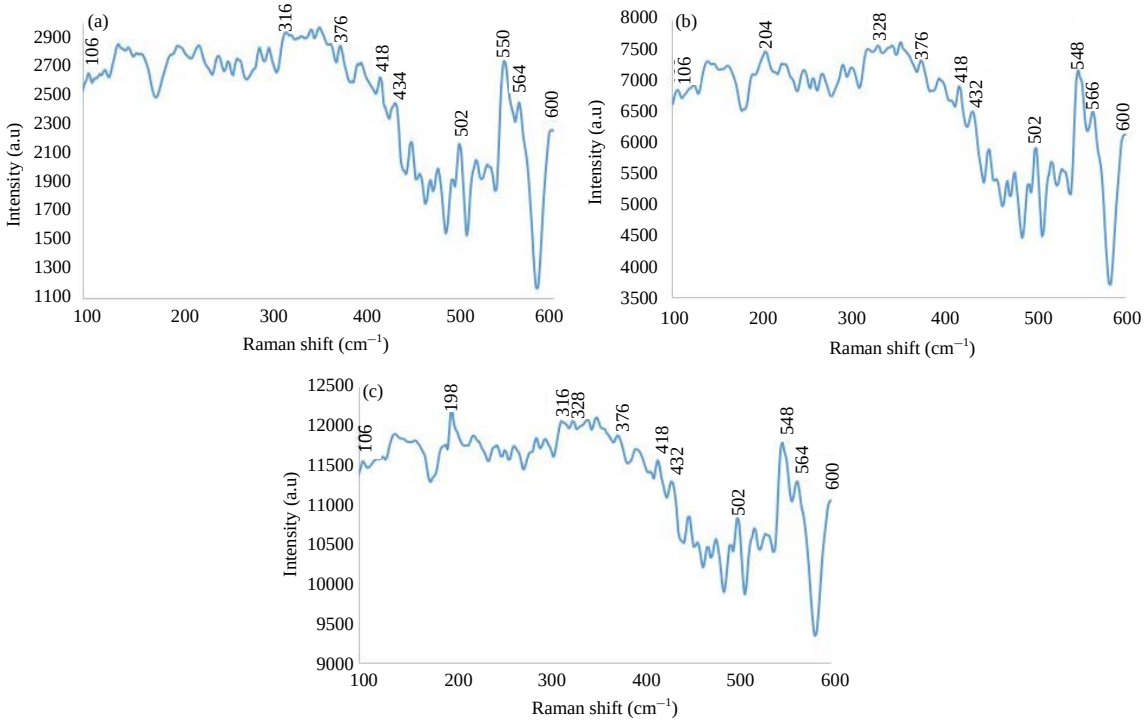

Fig. 8(a-c): Raman spectra of the ZnO film samples for different Zn film substrate temperatures, (a) T_{sub_RT}, (b) $T_{sub\_100°C}$ and (c) $T_{sub\_150°C}$

Evidently the samples exhibit similar scattering peaks, indicating identical crystal structures irrespective of Zn film precursor substrate temperature, confirming observations from XRD analysis on c/a ratio and bond length L values.

CONCLUSION

The effect of metallic Zn precursor substrate temperature on the morphological, the structural optical and vibrational properties ZnO thin films synthesized by thermal oxidation of the metallic Zn films was investigated. There is significant modification in morphology showing different nanostructures at different Zn precursor substrate temperatures. Lower Zn film substrate temperature show high deviation from ZnO stoichiometry of the synthesised ZnO films which improved significantly at higher Zn precursor substrate temperature due to more effective path for oxygen diffusion and reaction with metallic Zn film deposited at elevated substrate temperature. The XRD results revealed that all the ZnO films show dominant (011) orientation of wurtzite structure with other identified peaks associated with Zn hexagonal results from un-oxidised zinc atoms that disappear at increased Zn metallic film substrate temperature. The transmittance improved from 64-77%, while band gaps improved from 2.35-3.30 eV at higher Zn substrate temperature, the lower values attributable to greater density of states near the conduction band resulting from oxygen vacancies. The characteristic wurtzite ZnO peaks of E_2^{low} are observed at 106 cm^{-1} for the three samples showing a blue shift. Raman peaks between 570 and 590 cm^{-1} reveal structural defects attributed to oxygen vacancy, Zn insterstitial and their combination. The XRD and Raman analysis suggests the synthesised ZnO films have identical crystal structures irrespective of Zn precursor substrate temperature. The precursor Zn film substrate temperature show significant effect on morphology, nanostructure shape and stoichiometry of the ZnO films. The control of the growth morphology and stoichiometry of ZnO may have an impact in optoelectronic applications.

ACKNOWLEDGMENTS

The authors will like to acknowledge the Physics Advanced Laboratory, Sheda Science and Technology Complex (SHESTCO), Abuja, Nigeria for synthesis of the samples and the Microelectronics and Nanotechnology Shamsuddin Research Centre (MiNT-SRC) of the Universiti Tun Hussein Onn malaysis for FESEM, XRD and Raman characterization.

REFERENCES

1. Segets, D., J. Gradl, R.K. Taylor, V. Vassilev and W. Peukert, 2009. Analysis of optical absorbance spectra for the determination of ZnO nanoparticle size distribution, solubility and surface energy. ACS Nano, 3: 1703-1710.
2. Bacaksiz, E., M. Parlak, M. Tomakin, A. Ozcelik, M. Karakiz and M. Altunbas, 2008. The effects of zinc nitrate, zinc acetate and zinc chloride precursors on investigation of structural and optical properties of ZnO thin films. J. Alloys Compd., 466: 447-450.
3. Wang, J., J. Cao, B. Fang, P. Lu, S. Deng and H. Wang, 2005. Synthesis and characterization of multipod, flower-like and shuttle-like ZnO frameworks in ionic liquids. Mater. Lett., 59: 1405-1408.
4. Chaari, M. and A. Matoussi, 2012. Electrical conduction and dielectric studies of ZnO pellets. Physica B: Condensed Matter, 407: 3441-3447.
5. Ozgur, U., Y.I. Alivov, C. Liu, A. Teke and M.A. Reshchikov *et al*., 2005. A comprehensive review of ZnO materials and devices. J. Applied Phys., Vol. 98. 10.1063/1.1992666.
6. Bhattacharyya, S. and A. Gedanken, 2008. A template-free, sonochemical route to porous ZnO nano-disks. Microporous Mesoporous Mater., 110: 553-559.
7. Ludi, B. and M. Niederberger, 2013. Zinc oxide nanoparticles: Chemical mechanisms and classical and non-classical crystallization. Dalton Trans., 42: 12554-12568.
8. Lu, Y.J., H.F. Li, C.X. Shan, B.H. Li, D.Z. Shen, L.G. Zhang and S.F. Yu, 2014. Improved performance of ZnO light-emitting devices by introducing a hole-injection layer. Opt. Express, 22: 17524-17531.
9. Wang, Y., J. Liu, L.L. Liu and D.D. Sun, 2012. Enhancing stability and photocatalytic activity of ZnO nanoparticles by surface modification of graphene oxide. J. Nanosci. Nanotechnol., 12: 3896-3902.
10. Kumar, R., G. Kumar, O. Al-Dossary and A. Umar, 2015. ZnO nanostructured thin films: Depositions, properties and applications-a review. Mater. Express, 5: 3-23.
11. Wu, D., Z. Bai and K. Jiang, 2009. Temperature induced hierarchical growth of ZnO microcrystal. Mater. Lett., 63: 1057-1060.
12. Mihailova, I., V. Gerbreders, E. Tamanis, E. Sledevskis, R. Viter and P. Sarajevs, 2013. Synthesis of ZnO nanoneedles by thermal oxidation of Zn thin films. J. Non-Crystalline Solids, 377: 212-216.
13. Lin, Y., J. Xie, H. Wang, Y. Li and C. Chavez *et al*., 2005. Green luminescent zinc oxide films prepared by polymer-assisted deposition with rapid thermal process. Thin Solid Films, 492: 101-104.
14. Hu, S.Y., Y.C. Lee, J.W. Lee, J.C. Huang, J.L. Shen and W. Water, 2008. The structural and optical properties of ZnO/Si thin films by RTA treatments. Applied Surface Sci., 254: 1578-1582.
15. Li, C., X. Li and D. Wang, 2015. Fabrication of ZnO Thin Film and Nanostructures for Optoelectronic Device Applications. In: Oxide Thin Films, Multilayers and Nanocomposites, Mele, P., T. Endo, S. Arisawa, C. Li and T. Tsuchiya (Eds.). Springer, Cham, Switzerland, ISBN: 9783319144788, pp: 239-272.
16. Petrov, I., P. B. Barna, L. Hultman and J.E. Greene, 2003. Microstructural evolution during film growth. J. Vacuum Sci. Technol. A, 21: S117-S128.
17. Lee, Y.E., J.B. Lee, Y.J. Kim, H.K. Yang, J.C. Park and H.J. Kim, 1996. Microstructural evolution and preferred orientation change of radio-frequency-magnetron sputtered ZnO thin films. J. Vacuum Sci. Technol. A, 14: 1943-1948.
18. Guo, C.F., Y. Wang, P. Jiang, S. Cao, J. Miao, Z. Zhang and Q. Liu, 2008. Zinc oxide nanostructures: Epitaxially growing from hexagonal zinc nanostructures. Nanotechnology, Vol. 19, No. 44. 10.1088/0957-4484/19/44/445710.
19. Gui, Y., C. Xie, Q. Zhang, M. Hu, J. Yu and Z. Weng, 2006. Synthesis and characterization of ZnO nanostructures by two-step oxidation of Zn nano- and microparticles. J. Crystal Growth, 289: 663-669.
20. Snyder, R.L., 1999. X-Ray Diffraction. In: X-Ray Characterization of Materials, Lifshin, E. (Ed.). Chapter 1, Wiley-VCH, Germany, ISBN: 9783527296576, pp: 1-103.
21. Ong, H.C., A.X.E. Zhu and G.T. Du, 2002. Dependence of the excitonic transition energies and mosaicity on residual strain in ZnO thin films. Applied Phys. Lett., 80: 941-943.
22. Ambacher, O., J. Majewski, C. Miskys, A. Link and M. Hermann *et al*., 2002. Pyroelectric properties of Al(In)GaN/GaN hetero and quantum well structures. J. Phys.: Condensed Matter, Vol. 14, No. 23. 10.1088/0953-8984/14/13/302
23. Zhang, X.Y., Z.W. Chen, Y.P. Qi, F. Yan and Z. Liang *et al*., 2007. Ab initio comparative study of zincblende and wurtzite ZnO. Chin. Phys. Lett., Vol. 24. 10.1088/0256-307X/24/4/051
24. Kong, X.Y., Y. Ding, R. Yang and Z.L. Wang, 2004. Single-crystal nanorings formed by epitaxial self-coiling of polar nanobelts. Science, 303: 1348-1351.
25. Urbach, F., 1953. The long-wavelength edge of photographic sensitivity and of the electronic absorption of solids. Phys. Rev., 92: 1324-1326.
26. Studenyak, I., M. Kranjec and M. Kurik, 2014. Urbach rule in solid state physics. Int. J. Optics Applic., 4: 76-83.
27. Cody, G.D., 1992. Urbach edge of crystalline and amorphous silicon: A personal review. J. Non-Crystalline Solids, 141: 3-15.
28. Ziabari, A.A. and F.E. Ghodsi, 2012. Growth, characterization and studying of sol-gel derived CdS nanoscrystalline thin films incorporated in polyethyleneglycol: Effects of post-heat treatment. Solar Energy Mater. Solar Cells, 105: 249-262.
29. Klung, H.P. and L.E. Alexandar, 1974. X-ray Diffraction Procedures for Polycrystalline and Amorphous Materials. 2nd Edn., Wiley, New York, Pages: 966.

30. Buono-Core, G.E., G. Cabello, A.H. Klahn, R. Del Rio and R.H. Hill, 2006. Characterization of pure ZnO thin films prepared by a direct photochemical method. J. Non-Crystalline Solids, 352: 4088-4092.
31. Marquez, J.A.R., C.M.B. Rodriguez, C.M. Herrera, E.R. Rosas, O.Z. Angel and O.T. Pozos, 2011. Effect of surface morphology of ZnO electrodeposited on photocatalytic oxidation of methylene blue dye part I: Analytical study. Int. J. Electrochem. Sci., 6: 4059-4069.
32. Morkoc, H. and U. Ozgur, 2009. Zinc Oxide: Fundamentals, Materials and Device Technology. Wiley-VCH; Germany, ISBN-13: 978-3527408139, Pages: 488.
33. Guo, S., Z. Du and S. Dai, 2009. Analysis of Raman modes in Mn-doped ZnO nanocrystals. Physica Status Solidi (b), 246: 2329-2332.
34. Cusco, R., E. Alarcon-Llado, J. Ibanez, L. Artus, J. Jimenez, B. Wang and M.J. Callahan, 2007. Temperature dependence of Raman scattering in ZnO. Phys. Rev. B, Vol. 75. 10.1103/PhysRevB.75.165202
35. Damen, T.C., S.P.S. Porto and B. Tell, 1966. Raman effect in zinc oxide. Phys. Rev., 142: 570-574.
36. Zhang, R., P.G. Yin, N. Wang and L. Guo, 2009. Photoluminescence and Raman scattering of ZnO nanorods. Solid State Sci., 11: 865-869.
37. Wang, Z.L., 2008. Splendid one-dimensional nanostructures of zinc oxide: A new nanomaterial family for nanotechnology. ACS Nano, 2: 1987-1992.